Advances in quantum dots for classical and non-classical light sources

Invited Paper

Yasuhiko Arakawa, Satoshi Iwamoto, Satoshi Kako, Masahiro Nomura, and Denis Guimard

Research Center for Advanced Science and Technology, Institute for Nano Quantum Information Electronics, The University of Tokyo, 4-6-1 Meguro-ku, 153-8505 Tokyo, Japan

Received August 5, 2008

Recent advances in quantum dots (QDs) for classical and non-classical light sources are presented. We have established metal organic chemical vapor deposition (MOCVD) technology for InAs-based QD lasers at 1.3 μm and achieved ultralow threshold in QD lasers with photonic crystal (PhC) nanocavity. In addition, single photon emitters at 1.55 μm, GaN-based single photon sources operating at 200 K, and high-Q PhC nanocavity have been demonstrated.

OCIS codes: 250.0250, 250.5590, 160.5298.
doi: 10.3788/COL20080610.0718.

1. Introduction

Following Esaki's pioneering work on superlattices and quantum wells, the concept of quantum dots (QDs) was proposed by Arakawa and Sakaki in 1982 for application to semiconductor lasers with the theoretical prediction of temperature insensitive threshold current characteristics[1−3]. Full confinement of electrons in the QDs has brought up unique features of artificial atoms, such as discrete energy states and correlation effects due to spin/charging effects. This has resulted in a wide variety of experimental investigations into semiconductor physics and device applications.

Owing to development of the self-assembled growth technique of high-quality QDs[4], high speed 1.3-μm QD lasers with temperature-insensitive characteristics were demonstrated by the University of Tokyo and Fujitsu[5]. This successful achievement led to the launch of a curve-out type of venture company called QD Lasers Corporation in 2006. The QD lasers will be in a real commercial market in the quite near future for telecom applications.

In addition to photonic device applications based on an ensemble of many QDs, single or coupled QDs are promising for quantum information devices, such as single photon emitters and quantum-bit devices. In the quantum information devices, single photon-electron interaction and quantum entangled states are manipulated based on electron spins, charges, and nuclear spins. Even for classical light sources, a single dot with photonic nanocavities has been led to the concept of "single artificial atom lasers". Recently, we have achieved a quasi-single dot laser with a photonic crystal (PhC) nanocavity[6].

A major application proposed for non-classical light sources such as single-photon emitters is quantum cryptography communication. This is a scheme for encoding bits of information in the states of single photons. Regarding single photon emission, there have already been various demonstrations using single atoms, single molecules, and single QDs. In particular, semiconductor QDs are the most promising for practical applications. However, the experiments on single photon emission from QDs were mainly at liquid helium temperature and emitting light was at the wavelength less than 1 μm. Recently, emission of single-photon pulses in the C-band (1.55-μm band: the highest transmittance in optical telecommunication bands) from a single InAs/InP QD was demonstrated[7,8]. Moreover, by establishing growth technology of high-quality GaN/AlN QDs, triggered single-photon emission at higher temperatures up to 200 K was demonstrated, which is the highest temperature in all semiconductor single photon emitters[9].

The QDs are promising for realizing various quantum information devices such as entangled photon pair generators and quantum logic gate. Moreover, the QDs can be applied to bio-markers and solar energy technologies. As indicated in Fig. 1, through the investigation of physics and device technologies of the QDs, we could contribute to "green society" which can be realized by highly efficient IT and global eco-technologies.

In this presentation, we discuss prospects of QDs focusing on our advances in classical and non-classical sources. The presentation includes our recent progress in QD lasers at 1.3 μm grown by metal organic chemical vapor deposition (MOCVD), ultralow threshold QD lasers

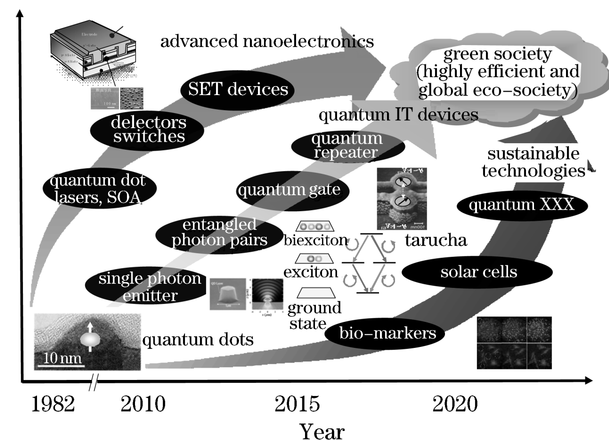

Fig. 1. QDs toward green society.

 © 2008 Chinese Optics Letters

with PhC nanocavities, and GaN-based QDs for single photon emitters operating at the highest temperatures.

2. MOCVD-grown QD lasers

The commercialization of QD lasers for the telecom market requires the fabrication of efficient lasers emitting at 1.3 μm, via a process suitable for production. Here, we report the fabrication of the first QD lasers above 1.3 μm, grown by MOCVD. This was achieved due to the beneficial effects of the antimony-mediated growth of InAs/Sb:GaAs QDs. Because of their theoretically predicted properties, such as low threshold current density and high temperature stability[1], self-assembled InAs/GaAs QDs are attractive candidates for emitters at the telecommunication wavelength of 1.3 μm. Lasing at 1.3 μm has been extensively reported for InAs/GaAs QDs grown by molecular beam epitaxy (MBE)[10]. Because of the advantages of MOCVD, such as high throughput and lower maintenance costs, the fabrication of QD lasers by this process would help QD lasers to find commercialization. However, until very recently, there has been no report of lasing at, or above, 1.3 μm from InAs/GaAs QDs grown by MOCVD. These limitations lied in the difficulty to grow high-density QDs with sufficient gain from the ground state (GS) transition, and in the high temperature requiring for the growth of the AlGaAs upper cladding layer (UCL), whcih induced a significant blueshift.

Recently, we showed that the antimony-mediated growth of InAs/Sb:GaAs QDs could break these deadlocks[11]. The density of InAs/Sb:GaAs QDs can be controlled by the amount of antimony, and be increased up to 10^{11} cm^{-2}, as illustrated in Fig. 2. Antimony modifies the kinetic and thermodynamics of the growth process. Besides, the InAs/Sb:GaAs QDs yield unchanged emission wavelength upon annealing up to 630 − 640 °C, unlike conventional InAs QDs grown on GaAs alone. With regards to laser fabrication, this allows the achievement of both flat spacer layers and AlGaAs UCL of high structural quality, with emission maintained above 1.3 μm.

We demonstrated for the first time GS lasing above 1.3 μm from MOCVD-grown GaAs-based QD lasers[12], with record values of maximum GS modal gain of 12.5

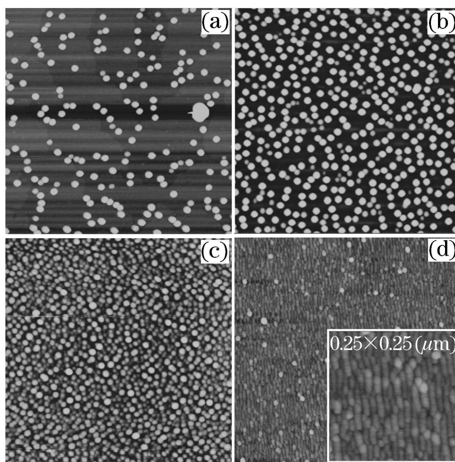

Fig. 2. 1 × 1 (μm) images of InAs QDs grown on (a) GaAs and Sb:GaAs, (b), (c), and (d) with increasing amount of Sb.

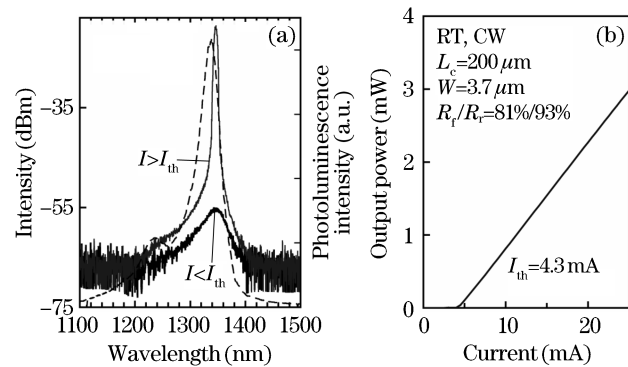

Fig. 3. (a) RT EL spectra (solid lines) of fabricated ten-stacked QD layer laser just below ($I < I_{\rm th}$) and above threshold ($I > I_{\rm th}$), and RT photoluminescence spectrum of the QD active region (dashed line); (b) L-I characteristics under CW operation at RT.

and 19.3 cm^{-1} for five- and ten-stack lasers, respectively. Figures 3(a) and (b) show respectively the electroluminescence (EL) lasing spectra, below and above threshold, and the output power-current (L-I) characteristics of a ten-stack narrow stripe laser structure measured at room temperature (RT) under continuous-wave (CW) operation, with cavity length of 200 μm and highly-reflective coatings (81%/93%). The threshold current $I_{\rm th}$ is 4.3 mA. Lasing occurs at the wavelength of 1.35 μm, which corresponds to the GS emission.

We believe these results open promising prospects for the commercialization of QD lasers. Next targets are the improvement of the laser characteristics, such as the decrease of the threshold current density and the increase of the modal gain.

3. Toward single QD lasers — QD lasers with PhC nanocavity

The physics in a coupling system of a PhC nanocavity and QDs are subjected to the law of cavity quantum electrodynamics. Therefore, highly efficient light-matter coupling phenomena can be observed. These physics, not only high academic interest, can be applied to ultralow power consumption coherent light emitters. In this article, we demonstrate GaAs QD-based CW PhC nanocavity laser with an ultralow threshold. Figure 4 shows schematic illustration and scanning electron microscope (SEM) images of a fabricated PhC structure. Further details about PhC fabrication can be found elsewhere.

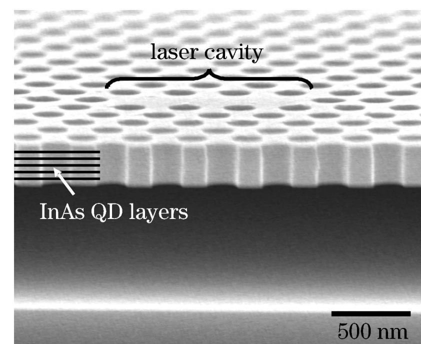

Fig. 4. Scanning electron micrograph of the PhC nanocavity structure.

The PhC nanocavity laser is considered one of the best candidates for ultralow threshold lasers due to their small mode-volume of the order of cubic wavelength and high quality factor Q. The first PhC laser was reported with multi-quantum well (MQW) structures in 1999[13]. PhC lasers with QDs as the gain material have been more difficult devices to construct due to their inherently lower modal gain. In the past decade, some groups have been challenging to achieve laser operation in PhC nanocavities with QD gain material. Recently, CW laser operation at low temperature[14] and RT[15] has been reported in PhC nanocavities with QDs. The light-in versus light-out plots of these lasers show soft turn-on behavior around the laser thresholds, while conventional lasers show pronounced kinks. This is because the spontaneous emission efficiently couples to the lasing mode in such lasers. The spontaneous emission coupling factor β is the spontaneous emission rate into the lasing mode divided by the total spontaneous emission rate. A large value of β results in efficient lasing and reduces the lasing threshold. Therefore, many groups have been striving to achieve high-β lasers.

Three-dimensional (3D) photon confinement is obtained by fabricating the PhC slab structure with a nanocavity composed of three missing air holes as shown in Fig. 3. The sample was grown on a (100) GaAs substrate by MBE, and then the PhC structures were fabricated using an electron beam lithography, dry and wet etching processes. The air-bridged structure was obtained by etching with HF acid of an AlGaAs sacrificial layer, which was grown between the GaAs substrate and the GaAs slab layer. The slab layer contains five InAs self-assembled QD layers. The density of the QDs is 2×10^{10} cm^{-2} for each QD layer, and $\sim$ 800 QDs are located in the nanocavity. Further details of the sample and fabrication processes were reported in our previous paper[16]. The structural parameters of the sample are: lattice constant $a = 355$ nm and radius of the air hole $r = 96$ nm. The first and third nearest air holes at both ends of the cavity were shifted outward by $0.15a$.

Optical measurements were performed with a micro-photoluminescence (μ-PL) setup at RT using a CW laser diode ($\lambda = 785$ nm) as the excitation emitter. The pump laser beam was focused on the sample surface by a microscope objective, and was positioned on the PhCs using piezo-electric nanopositioners.

The lasing was observed at the lowest-order cavity mode at 1.33 μm, which is located near the PL peak from the excitonic state of the InAs QD ensemble. The conventional estimation of the lasing threshold, which is obtained by extrapolation of the line to zero output power, yields an irradiated threshold excitation power of $\sim$ 2.5 μW, about 375 nW in the estimated absorbed power (Fig. 5). The absorbed power was estimated by considering a surface reflectivity of $\sim$ 30%, the thickness of the slab layer of 250 nm, and an approximate absorption coefficient of 10000 cm^{-1}. From these values, the absorbed power in the slab layer is estimated to be $\sim$ 15% of the pump power. However, the spatial overlap of the pump beam and the cavity was not considered, because the inflow of the photo-carriers into the cavity is unknown. Recently, RT CW lasing with an extremely low threshold of 1 μW absorbed pump power

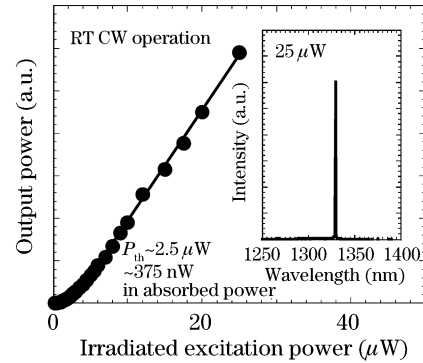

Fig. 5. L-L plot of the PhC nanocavity CW laser at RT. Inset shows the lasing spectrum.

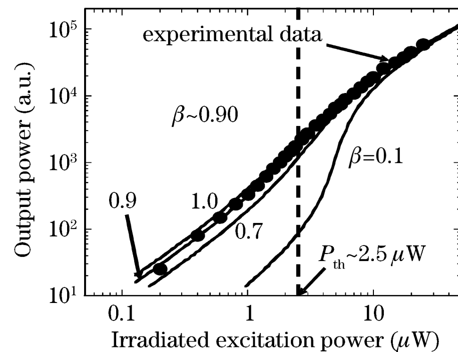

Fig. 6. Experimental L-L plot in logarithmic scale and fitting curves for various β.

in AlGaAs microdisks with InAs QD gain material has been reported. The absorbed pump power of our PhC nanocavity laser is comparable to these microdisk lasers. To the best of our knowledge, this is the smallest CW laser with QD gain material that operates at RT and has the smallest threshold pump power.

The L-L curve in Fig. 6 shows no sharp threshold but a very soft turn-on of the laser operation. This behavior is typical for a laser with a large β. The value of β of our laser was estimated by fitting the experimental L-L plot by theoretical L-L curves calculated using rate equations. Figure 6 shows the L-L plot in the logarithmic scales in both axes. The best fit has been found for $\beta = 0.9$ with $g_0 = 1 \times 10^5$ cm^{-1}. A laser with $\beta = 1$ is expected to have a threshold-less behavior. However, the simulated L-L curve with $\beta = 1$ shows a very obscure kink. This is because the nonradiative recombination is not negligible at RT, especially in the low excitation power regime, which corresponds to the subthreshold regime for a lower-β laser.

The value of Q was estimated from the coherence length measurement. The coherence length at the transparent pump power of 2.5 μW was 3.7 cm. The calculated spectral width $\delta\nu$ is $\sim$ 2.6 GHz and the value of Q is $\sim$ 87000, which gives a photon lifetime of $\tau_{\rm p} \sim 62$ ps[8]. The relatively large $\delta\nu$ may be attributed to the fact that the QD ensemble is an inhomogeneous gain material.

A combination of such a high quality PhC nanocavity and ideal single QD can realize single artificial atom laser. This solid state system will provide us stable test bed of cavity quantum electrodynamics.

4. Nitride-based single photon emitters operating at a high temperature

Nitride semiconductors have emerged in the last decade as important materials for blue and ultraviolet (UV) light-emitting devices. For quantum information processing applications, nitride QD structures open a new spectral region of blue and UV for single-photon emitters. III-nitride QDs are promising materials for a short-wavelength solid phase extraction (SPE) expected as a key device for satellite-based quantum information communication. Recently, we have performed single dot spectroscopy[17] and basic photon correlation studies on hexagonal GaN/AlN QDs[18]. These QDs could allow for high-temperature operation because of strong quantum confinement effects, large optical phonon energies, and the fact that they comprise binary materials. We have observed PL from a single GaN QDs even at RT. In this section, we present GaN QD single-photon emitter which has the capability of high-temperature operation, and AlN PhC nanocavities which have potential ability to improve the performance.

4.1. Triggered single-photon emission

We have grown our GaN QD sample by MOCVD, and have developed the growth technique to control the size and density of the GaN QDs embedded by AlN[19]. Typical structure of our GaN QDs is a truncated hexagonal pyramidal shape. Hexagonal nitride semiconductor heterostructures are quite unique in terms of the existence of a strong built-in electric field due to a spontaneous polarization difference and a strain-induced piezoelectric polarization. We have investigated this effect on GaN/AlN QDs by means of time-resolved PL measurement (TRPL) and theoretical calculation[20]. We have found that a PL decay time and an emission wavelength of QDs strongly increase with increasing the size of the QDs, which could be attributed to reduce oscillator-strength and quantum-confined Stark effects due to the strong built-in electric field induced by both the piezoelectric field in the GaN QDs.

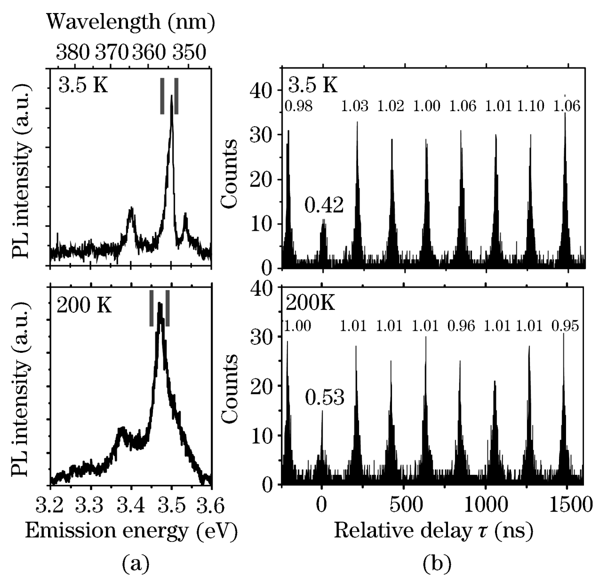

Fig. 7. (a) PL spectra under pulsed excitation. The spectral regions between the solid lines indicate approximately the portion of the spectrum that reaches the detectors after filtering; (b) histograms under pulsed excitation. The numbers printed above the peaks give the normalized peak areas after correcting for the detector dark counts.

To demonstrate triggered single-photon generation, we have measured the second-order coherence function $g^{(2)}(\tau)$ under pulsed wetting-layer excitation with the repetition rate of 4.74 MHz[18,21]. We selected the single-exciton emission peak with spectral filters as shown in Fig. 7(a). The auto-correlation histograms at the temperatures of 3.5 and 200 K are shown in Fig. 7(b). The $\tau = 0$ peak corresponds to events where two photons were detected following the same excitation pulse. A clear antibunching effect is observable at temperatures up to 200 K. We obtain $g^{(2)}[0] = 0.42$ for the temperature of 3.5 K, indicating that the two-photon probability is reduced to 0.42 times that for an equivalent Poisson-distributed emitter. The $g^{(2)}[0]$ is the normalized coincidences counts (peak area) for $-T/2 < t < T/2$, where T is the repetition period of the pulsed excitation. At 200 K, the two-photon probability increased slightly to 0.53. This small degradation can be attributed to contamination from biexciton emission, due to the inability to spectrally separate the emission lines. Although the integrated intensity shows little variation up to 200 K, the exciton and biexciton emission peaks are no longer well resolved at 200 K as shown in Fig. 7(a), in contrast to the measurements at 3.5 K. Therefore a narrow spectral diffusion linewidth and a large separation energy between exciton and biexciton lines are crucial for obtaining small $g^{(2)}[0]$ values at higher temperatures.

Presently, despite of this potential for high efficiency up to 250 K, the highest operation temperature is restricted to 200 K. One of the obstacles is the reduction of the emission efficiency above 200 K, requiring a longer integration time to complete the measurement. We found that such long periods of irradiation by intense UV pulses degraded the sample surface, especially in processed regions, before measurements could be completed. This limitation, however, could be overcome in the future by means of, for instance, using excitation pulses with lower photon energy or introducing a protection layer on the top of processed sample.

4.2. AlN photonic crystal

Previous efforts of nitride-based PhCs have been mainly concentrated on improvement of extraction efficiency of short wavelength light emitting diodes[22,23] and only few reports have presented PhC nanocavity exhibiting the cavity modes in blue/violet region[24]. To fabricate the nitride-based PhC nanocavities with GaN/AlN QDs, we have investigated AlN PhC nanocavities[25]. We first prepared triangular lattice PhC patterns by electron beam (EB) lithography and ion etching (ICP-RIE). Since the refractive index of SiC (2.83) is higher than that of AlN (2.2), the SiC substrate must be removed to confine optical modes in the AlN PhC nanocavity. We employed photoelectrochemical wet etching techniques to partially lift-off the epitaxial layers from the substrate.

Figure 8 illustrates the micro-PL spectra of nanocavities consist of seven missing holes (L7 nanocavity) with different periodicities. Sharp luminescence lines attributed to the cavity modes were observed from all the

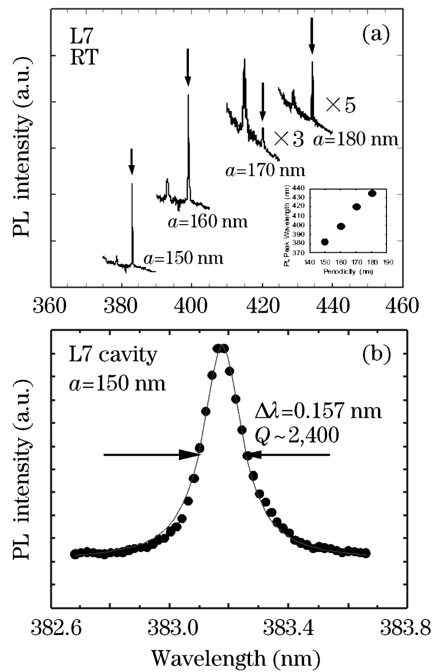

Fig. 8. Micro-PL spectra of the nanocavities. (a) Periodicity dependence of the lowest-order modes of L7 cavities; (b) Loretzian fitting result of the peak of the 150-nm-period cavity.

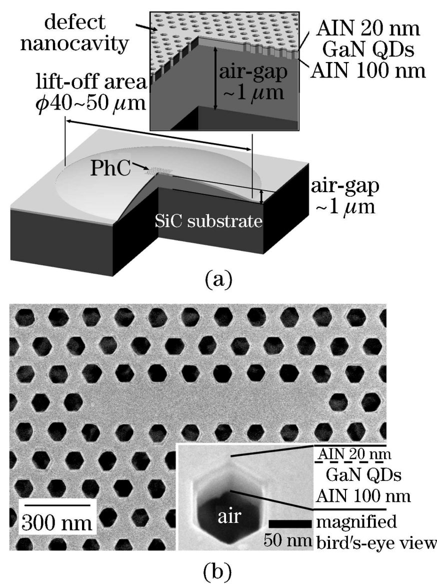

Fig. 9. (a) Illustrations of cross-sectional cut of the convex-shaped air-bridge PhC structure formed by partially lift-off epitaxial III-nitride layers. Inset shows a magnification around air-bridge PhC region; (b) SEM images of fabricated PhC nanocavity with periodicity of 150 nm. Inset is a bird's eye view of an air hole. Abrupt vertical etching profile and hexagonal shape of the holes are attributed to crystallographic-orientation dependent chemical etching.

cavities. In Fig. 8(a), arrows indicate the positions of the lowest-order modes. Peak wavelengths of the lowest-order cavity modes shifted toward a longer wavelength as the periodicity was increased as shown in the inset of the figure. From Lorentzian fitting analysis of the cavity mode of the 150-nm-period L7 cavity, linewidth of 0.157 nm (1.33 meV) was confirmed, as shown in Fig. 8(b). The Q-factor of this cavity is then estimated to be more than 2400. To the best of our knowledge, this is the highest Q-factor ever reported in nitride PhC. Figure 9 shows the illustrations of cross-sectional cut of the convex-shaped air-bridge PhC structure formed by partially lift-off epitaxial III-nitride layers and SEM images of fabricated PhC nanocavity with periodicity of 150 nm.

5. Conclusion

We have discussed recent advances in InAs-based QD devices including highly temperature-sable QD lasers, ultralow threshold power in nearly-single dot nanocavity lasers, and single photon emitters at 1.55 μm. In addition, GaN-based nanophotonic devices such as single photon emitters operating at 200 K and PhC nanocavity have been also discussed.

This work was supported by Special Coordination Funds for Promoting Science and Technology. The author would like to thank M. Ishida, Y. Nakata at the University of Tokyo as well as S. Hirose, S. Okumura, K. Takemoto, M. Takatsu, N. Yokoyama, M. Ekawa, N. Harada, N. Hatori, H. Sudo, T. Yamamoto, and M. Sugawara at Fujitsu laboratories for helpful discussion and continuous support. Y. Arakawa's e-mail address is arakawa@iis.u-tokyo.ac.jp.

References

1. Y. Arakawa and H. Sakaki, Appl. Phys. Lett. **40,** 939 (1982).
2. Y. Arakawa and A. Yariv, IEEE J. Quantum Electron. **22,** 1887 (1986).
3. Y. Arakawa, Solid-State Electron. **37,** 523 (1994).
4. L. Goldstein, F. Glas, J. Y. Marzin, M. N. Charasse, and G. Le Roux, Appl. Phys. Lett. **47,** 1099 (1985).
5. K. Otsubo, N. Hatori, M. Ishida, S. Okumura, T. Akiyama, Y. Nakata, H. Ebe, M. Sugawara, and Y. Arakawa, Jpn. J. Appl. Phys. **43,** L1124 (2004).
6. M. Nomura, S. Iwamoto, and Y. Arakawa, (to be published).
7. K. Takemoto, Y. Sakuma, S. Hirose, T. Usuki, N. Yokoyama, T. Miyazawa, M. Takatsu, and Y. Arakawa, Jpn. J. Appl. Phys. **43,** L993 (2004).
8. T. Miyazawa, K. Takemoto, Y. Sakuma, S. Hirose, T. Usuki, N. Yokoyama, M. Takatsu, and Y. Arakawa, Jpn. J. Appl. Phys. **44,** L620 (2005).
9. S. Kako, C. Santori, K. Hoshino, S. Goetzinger, Y. Yamamoto, and Y. Arakawa, Nature Material **5,** 887 (2006).
10. D. L. Huffaker, G. Park, Z. Zou, O. B. Shchekin, and D. G. Deppe, Appl. Phys. Lett. **73,** 2564 (1998).
11. D. Guimard, M. Nishioka, S. Tsukamoto, and Y. Arakawa, Appl. Phys. Lett. **89,** 183124 (2006).
12. D. Guimard, M. Ishida, S. Tsukamoto, M. Nishioka, Y. Nakata, H. Sudo, T. Yamamoto, M. Sugawara, and Y. Arakawa, Appl. Phys. Lett. **90,** 241110 (2007).
13. O. Painter, R. K. Lee, A. Scherer, A. Yariv, J. D. O'Brien, and P. D. Dapkus, Science **284,** 1819 (1999).
14. S. Strauf, K. Hennessy, M. T. Rakher, Y.-S. Choi, A. Badolato, L. C. Andreani, E. L. Hu, P. M. Petroff, and D. Bouwmeester, Phys. Rev. Lett. **96,** 127404 (2006).
15. M. Nomura, S. Iwamoto, K. Watanabe, N. Kumagai, Y. Nakata, S. Ishida, and Y. Arakawa, Opt. Express **14,** 6308 (2006).

16. M. Nomura, S. Iwamoto, K. Watanabe, N. Kumagai, Y. Nakata, S. Ishida, and Y. Arakawa, Phys. Rev. B **75,** 195313 (2007).
17. S. Kako, K. Hoshino, S. Iwamoto, S. Ishida, and Y. Arakawa, Appl. Phys. Lett. **85,** 64 (2004).
18. C. Santori, S. Götzinger, Y. Yamamoto, S. Kako, K. Hoshino, and Y. Arakawa, Appl. Phys. Lett. **87,** 051916 (2005).
19. M. Miyamura, K. Tachibana, and Y. Arakawa, Appl. Phys. Lett. **80,** 3937 (2002).
20. S. Kako, M. Miyamura, K. Tachiban, K. Hoshino, and Y. Arakawa, Appl. Phys. Lett. **83,** 984 (2003).
21. S. Kako, C. Santori, K. Hoshino, S. Götzinger, Y. Yamamoto, and Y. Arakawa, Nature Materials **5,** 887 (2006).
22. T. N. Oder, J. Shakya, J. Y. Lin, and H. X. Jiang, Appl. Phys. Lett. **83,** 1231 (2003).
23. L. Chen and A. V. Nurmikko, Appl. Phys. Lett. **85,** 3663 (2004).
24. Y.-S. Choi, K. Hennessy, R. Sharma, E. Haberer, Y. Gao, S. P. DenBaars, S. Nakamura, E. L. Hu, and C. Meier, Appl. Phys. Lett. **87,** 243101 (2005).
25. M. Arita, S. Ishida, S. Kako, S. Iwamoto, and Y. Arakawa, Appl. Phys. Lett. **91,** 051106 (2007).